INORGANIC CHEMISTRY FRONTIERS

RESEARCH ARTICLE

View Article Online
View Journal | View Issue

Cite this: *Inorg. Chem. Front.*, 2025, **12**, 6663

Electron-rich phenanthroline bearing N-heterocyclic imine substituents: synthesis, optical properties, metal coordination†

Jonas H. Franzen,[a] Xuequan Zhou,[b] Kelly Biv,[c] Alessandro Ajò,[b] Austin Mencke,[c] Lukas F. B. Wilm,[d] Michael Seidl,[a] Thomas S. Hofer,[a] Luisa De Cola,[b,e] Peter Brüggeller,[a] Mark E. Thompson *[c] and Fabian Dielmann *[a]

Received 22nd April 2025,
Accepted 7th June 2025

DOI: 10.1039/d5qi00957j

rsc.li/frontiers-inorganic

Polypyridines functionalized with π-donating groups constitute a class of electron-rich ligands with significant relevance in coordination chemistry and catalysis. The incorporation of strongly basic guanidinyl substituents, however, often introduces multiple binding sites, with coordination typically favoring the guanidyl nitrogen atoms. Herein, we report the synthesis and characterization of a new electron-rich 1,10-phenanthroline ligand featuring bulky NHI groups that define a well-structured coordination cavity. Protonation studies and the preparation of a zinc(II) complex reveal that Lewis acids preferentially coordinate at the phenanthroline nitrogen atoms rather than the NHI moiety. The electronic and photophysical properties of the new ligand and its complexes are explored through a combination of computational and experimental methods, demonstrating that its emission and absorption characteristics are highly sensitive to protonation, concentration, and metal coordination.

Introduction

N-heterocyclic imines (NHIs) are a class of cyclic guanidines characterized by an exocyclic imine function attached to a nitrogen-containing heterocycle. Their manifold accessibility takes root in the seminal synthetic protocols reported by Kuhn in 1995 and thereafter.[1–6] The use of NHIs as imine substituents or as anionic iminato ligands takes advantage of their capability to act as 4π or 2σ/4π donors, respectively, due to the allocation of electron density from the heterocycle to the exocyclic nitrogen atom (Fig. 1A).[7] The effective stabilization of a positive charge within the N-heterocycle renders NHIs stronger π donors compared to aliphatic guanidines. In addition, modifying the *N*,*N*′-substituents enables predictable steric control without compromising the potent donor properties. As a result, the coordination chemistry of NHIs towards main group and transition metal elements has been extensively investigated and reviewed in the past.[4–10]

While these characteristics have been pivotal for the stabilization and isolation of otherwise elusive low-valent main group species,[11–22] the exceptional electron-donating capacity of NHIs render them also particularly effective in generating electron-rich compounds.[23] For instance, our group has shown that guanidyl and NHI substituents produce superbasic phosphines when attached up to three times to a phosphorus centre.[24–27] We also demonstrated that decoration of porphyrins with NHIs can lead to improved selectivity in the electroreduction of CO_2.[28] Generally, the decoration of arenes with multiple π-donor substituents results in highly electron-rich π systems, which was utilized for the development of organic reducing agents,[29–37] dyes,[38,39] and redoxactive multidentate ligands.[40–43]

The influence of *para*-NHI substitution on the properties of pyridines has been studied using several descriptors, including the methyl cation affinity (MCA),[44–47] the molecular electrostatic potential (MESP) topology analysis,[48–51] and the Huynh electronic parameter (HEP).[52–54] Consistently, these parameters show that the electron-density at the pyridine N atom correlates with the π-donating ability of the NHI group

[a]*Institut für Allgemeine, Anorganische unt Theoretische Chemie, Leopod-Franzens-universität Innsbruck, Innrain 80-82, 6020 Innsbruck, Austria. E-mail: fabian.dielmann@uibk.ac.at*
[b]*Department of Biochemistry and Molecular Pharmacology, Istituto di Ricerche Farmacologiche Mario Negri, IRCCS, 20156 Milano, Italy. E-mail: luisa.decola@unimi.it*
[c]*Department of Chemistry, University of Southern California, Los Angeles, CA 90089, USA. E-mail: met@usc.edu*
[d]*Insitut für Anorganische und Analytische Chemie, Universität Münster, Corrensstraße 30, 48179 Münster, Germany*
[e]*Department of Pharmaceutical Science, DISFARM, Università degli Studi di Milano, Via C. Golgi 19, 20133 Milan, Italy*

†Electronic supplementary information (ESI) available: Synthetic procedures, NMR spectra, mass spectrometry data, crystallographic data, and computational details. CCDC 2420826–2420829. For ESI and crystallographic data in CIF or other electronic format see DOI: https://doi.org/10.1039/d5qi00957j

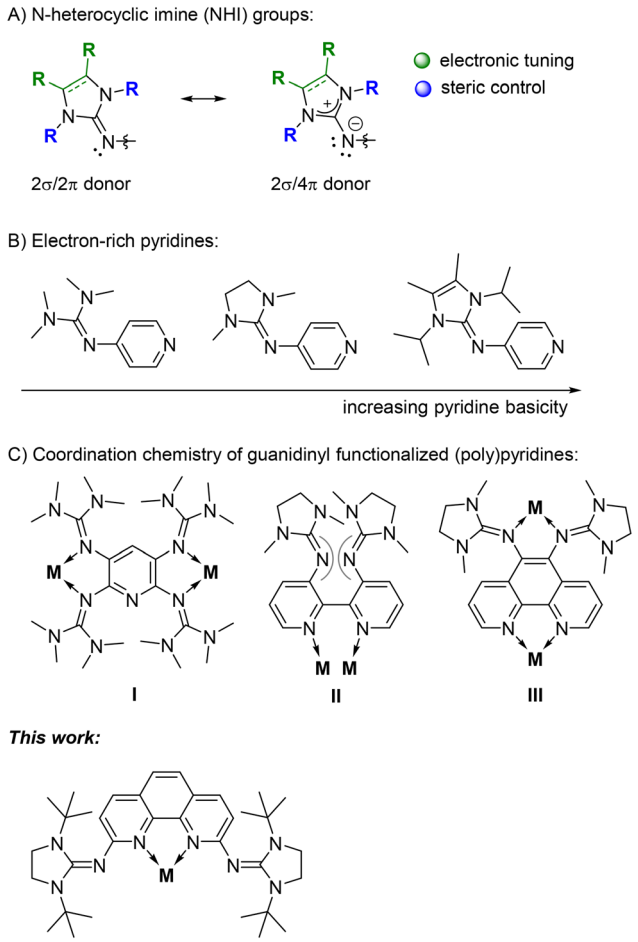

Fig. 1 (A) Mesomeric Lewis structure of the NHI scaffold. (B) and (C) Selected examples of electron-rich pyridine-based ligands with (cyclic) guanidyl substituents.

(Fig. 1B). This was experimentally demonstrated through the reversible formation of SO_2 and CO_2 adducts by the most basic pyridines which are not isolable using unsubstituted pyridine.[55–58] The Himmel group demonstrated that the incorporation of multiple guanidinyl groups into pyridine frameworks significantly increases the electron density of the pyridine ring and simultaneously generates ligands with multiple donor sites.[38,39,59–61] This is due to the fact that guanidines themselves are highly effective ligands in coordination chemistry.[62] As exemplified by compound **I**, guanidinyl groups frequently serve as the preferred coordination sites for transition metals **M** (Fig. 1C). Similarly, in the case of bipyridine derivative **II**, the guanidyl moieties compete with the pyridine nitrogen atoms for coordination to the metal center.[41] Moreover, Henkel and colleagues reported the synthesis of the 1,10-phenanthroline-based Janus head pro-ligand **III**, which can accommodate different transition metal centers at opposite ends of the molecule.[63,64]

In contrast, the parent 1,10-phenanthroline (phen) ligand is described as electron-deficient species with predominant π acceptor properties due to the large conjugated aromatic system and low-lying π* orbital.[65,66] Its rigidity causes the two N atoms to always be oriented *cis* to each other rendering phen an excellent chelating ligand[67] and the synthesis of coordination compounds incorporating almost every element of the periodic table has been realized.[65,68] Thus, the application of phen and its derivatives has been broadly explored over many areas of research such as materials chemistry,[69–73] medicinal chemistry,[74–79] catalysis,[80–87] and photochemistry.[88–95]

As part of our ongoing efforts to develop highly electron-rich ligands,[25,28,55] we report the synthesis and characterization of a 1,10-phenanthroline derivative bearing bulky *N*,*N*′-di-*tert*-butylimidazolin-2-ylidenamino substituents adjacent to the metal coordination site.

We hypothesize that, in contrast to the NHI carrying ligands **II** and **III**, this ligand will accommodate only a single metal center due to the rigid framework of the phenanthroline core and the steric hindrance provided by the *tert*-butyl groups. This design will allow for a detailed investigation of the effect of NHI substitution on the optical properties of 1,10-phenanthroline.

Results and discussion

Ligand and complex synthesis

The synthesis of the NHI-substituted 1,10-phenanthroline **1** was attempted in analogy to the reported procedure for the synthesis of N-heterocyclic imines.[96,97] Our group recently demonstrated the feasibility of this approach for pyridine based systems using 4-aminopyridine.[55] In fact, heating a suspension of 2,9-diamino-1,10-phenanthroline, *N*,*N*′-di-*tert*-butylimidazolin-2-chloroimidazolinium tetrafluoroborate[97,98] and KF at 90 °C for three days led to the selective formation of **1**·HBF$_4$ which was isolated after filtration and washing with water to remove excess KF in good yields (Scheme 1). **1**·HBF$_4$ is a bright yellow, bench-stable solid best soluble in polar organic solvents like DCM and MeCN. In the ^{1}H NMR spectrum, the acidic proton resonance of the **1**H$^+$ cation appears at high frequencies (CD_2Cl_2: 10.61 ppm, MeCN-d_3: 10.04 ppm) as a broad singlet indicating a dynamic process involving shut-

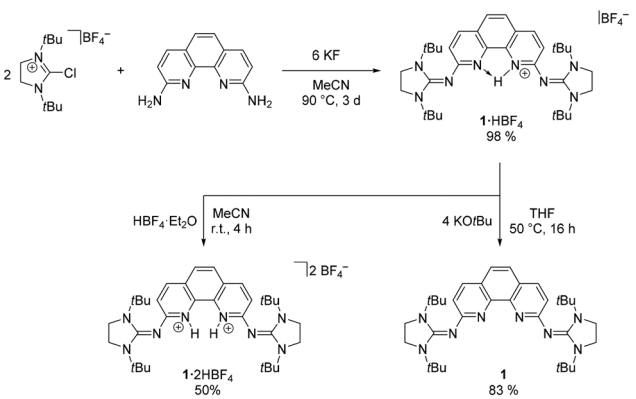

Scheme 1 Synthesis of **1**·HBF$_4$, **1**·2HBF$_4$ and the free ligand **1**.

tling of the proton. The sharp aromatic ^{1}H NMR resonances exhibit the typical splitting pattern for (protonated) 1,10-phenanthrolines of two doublets and one singlet.[99–101] Likewise, the NHI groups are chemically and magnetically equivalent and the methylene- and *tert*-butyl groups each appear as a singlet. Attempts to localize the acidic N–H proton using 2D and variable temperature NMR experiments remained unsuccessful (see ESI† for details). In symmetrically substituted phenanthroline ligands, the proton is bound between both N atoms.[69,102] A single-crystal X-ray diffraction (SCXRD) analysis of **1**·HBF$_4$ revealed that the proton is positioned on either of the two phenanthroline N atoms in a 1 : 1 ratio (see ESI† for details) (Fig. 2). The preferential protonation at the pyridine nitrogen rather than the NHI group is consistent with calculated proton affinities of various amino- and imino-substituted pyridines.[44,103]

DFT calculations at the B3LYP/6-31G(d,p)/SMD(DCM) level of theory confirm that the first protonation of **1** is energetically favored by 52.0 kJ mol^{-1} at a phenanthroline nitrogen atom compared to protonation at an imine group. The second protonation preferentially occurs at the imine nitrogen rather than the second phenanthroline nitrogen, with an energy advantage of 12.6 kJ mol^{-1} (see ESI† for details). DFT calculations reveal that the basicity of **1**, with a pK_{BH^+} value of 25.0 in acetonitrile (ACN), is significantly enhanced compared to pristine phenanthroline (pK_{BH^+} (ACN) = 13.7).[104] This places its basicity within the range of superbases such as DBU (pK_{BH^+} (ACN) = 24.1) and TBD (pK_{BH^+} (ACN) = 26.0).[105] This value was further validated by proton transfer experiments using a variety of bases, including DBU, TBD and the phosphazene base P$_1$-*t*Bu(pyrr)$_3$ (pK_{BH^+} (ACN) = 28.4)[106] (see ESI† for details). Experimentally, the second protonation was achieved using either HBF$_4$·Et$_2$O or [H(EtO)$_2$][B(C$_6$F$_5$)$_4$].[107] The ^{1}H NMR resonances of the resulting dication are significantly broadened, indicating the presence of several tautomers in solution. However, an SCXRD study of **1**·2HBF$_4$ revealed that, in the solid state, both protons are bound to the phenanthroline N atoms, forming hydrogen-bonding interactions with acetonitrile solvate molecules in the crystal lattice. Attempts to achieve further protonation and form [**1**·3H]$^{3+}$ using [H(OEt$_2$)$_2$][B(C$_6$F$_5$)$_4$] remained unsuccessful. In the ^{1}H NMR spectrum of the mixture, the resonances of [**1**·2H]$^{2+}$ and the acid were observed indicating that [**1**·2H]$^{2+}$ is less basic than Et$_2$O (see ESI† for more details). The free ligand **1** was isolated as an orange-to-red solid in good yields after deprotonation of **1**·HBF$_4$ with KO*t*Bu. **1** is soluble in polar organic solvents like MeCN and DCM, moderately soluble in

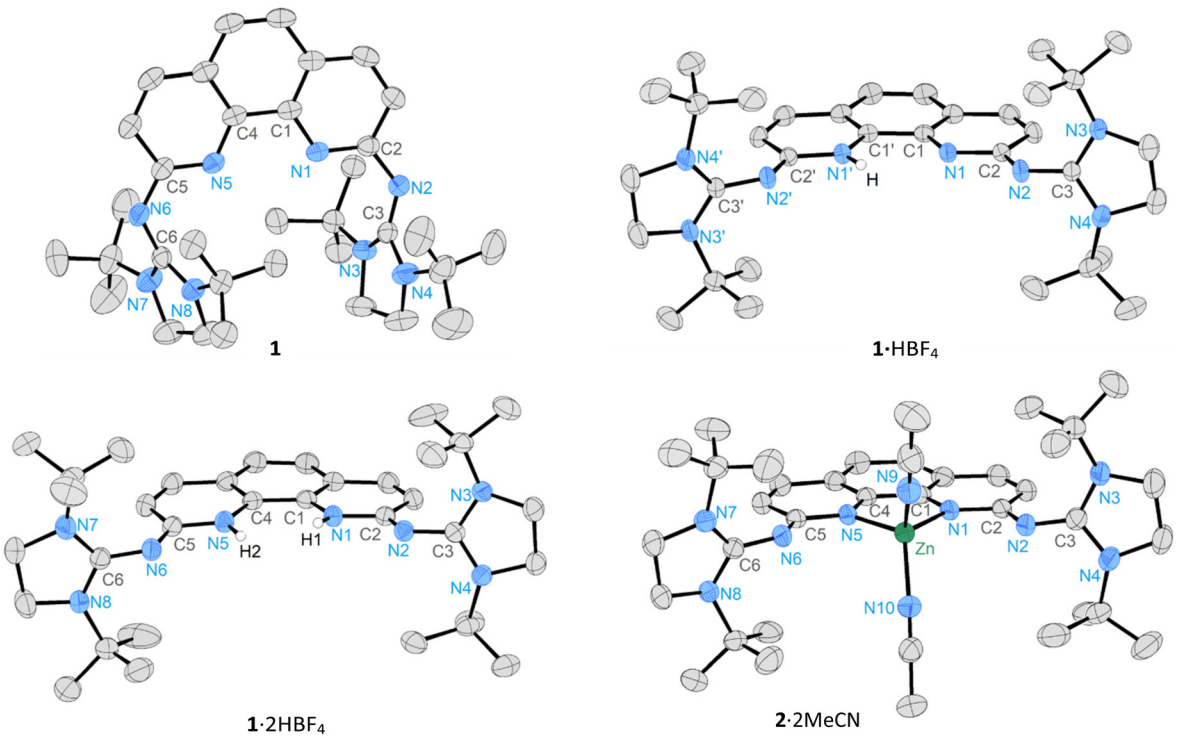

Fig. 2 Molecular structures of **1**, **1**·HBF$_4$ and **1**·2HBF$_4$ and **2**·2MeCN. Ellipsoids are set at 50% probability. Hydrogen atoms except for the N–H hydrogen atoms and counterions are omitted for clarity. Selected bond lengths (Å) and angles (°): **1**: C1–C4 1.451(2), C1–N1 1.363(2), N1–C2 1.339(1), C2–N2 1.348(2), N2–C3 1.307(2), C3–N3 1.367(2), C3–N4 1.367(2), N1–C2–N2 122.2(1), C2–N2–C3 130.3(1); **1**·HBF$_4$: C1–C1′ 1.423(3), C1–N1 1.366(3), N1–C2 1.352(3), C2–N2 1.326(3), N2–C3 1.332(3), C3–N3 1.350(3), C3–N4 1.354(3), N1–C2–N2 116.3(2), C2–N2–C3 126.2(2); **1**·2HBF$_4$: C1–C4 1.418(2), C1–N1 1.381(2), N1–C2 1.367(2), C2–N2 1.301(2), N2–C3 1.354(2), C3–N3 1.342(2), C3–N4 1.336(2), N1–C2–N2 116.1(1), C2–N2–C3 122.7(1); **2**·2MeCN: N1–Zn 1.984(2), N5–Zn 1.984(2), N9–Zn 1.972(3), N10–Zn 1.979(3), C1–C4 1.430(3), N1–C2 1.356(3), C2–N2 1.318(3), N2–C3 1.340(3), C3–N3 1.351(4), C3–N4 1.345(4), N1–C2–N2 116.5(2), C2–N2–C3 123.7(2), N1–Zn–N5 84.23(9), N9–Zn–N10 109.23(11).

Table 1 Selected averaged bond lengths and angles of **1** and **III**

	1	**III**
C_{phen}–N_{imine}	1.347(2) Å	1.398(2) Å
N_{imine}=C_{NHI}	1.314(2) Å	1.284(2) Å
C_{NHI}–N_{NHI}	1.364(2) Å	1.383(3) Å
C_{phen}–N_{imine}=C_{NHI}	130.3(1)°	126.3(2)°
N_{imine}=C_{NHI}–N_{NHI}	125.2(1)°	126.3(2)°
N_{NHI}–C_{NHI}–N_{NHI}	109.1(1)°	107.5(2)°

THF and toluene, and virtually insoluble in *n*-hexane or water. Nonspecific decomposition of **1** in $CDCl_3$ within minutes and in DCM-d_2 over the course of hours was observed by ^{1}H NMR spectroscopy reflecting the high basicity of **1**. Measured in C_6D_6, the phenanthroline ^{1}H NMR resonances of **1** appear at slightly higher frequencies (7.65 ppm, 7.21 ppm, 6.93 ppm) compared to those of the parent 1,10-phenanthroline (7.47 ppm, 7.07 ppm, 6.85 ppm).

The Zn^{II} complex **2**·2MeCN was prepared by treatment of **1** with $Zn(OTf)_2$ in MeCN at ambient temperature (Scheme 2). In contrast to phenanthroline complexes **III** (Fig. 1C), the use of an excess Zn^{II} did not lead to bimetallic complexes due to the close proximity of the bulky NHI groups to the coordination site in **1**. Protonation of **2**·2MeCN with $[H(OEt_2)_2][B(C_6F_5)_4]$ was accomplished, but it resulted in partial dissociation of the complex and the release of the cationic ligand **1**·$H(BC_6F_5)_4$. The solid-state structures of **1** and **2**·2MeCN were established by SCXRD studies (Fig. 2). For the free ligand **1**, the imidazole groups are staggered and rotated (Ø 65.3°) relative to the phenanthroline plane. In contrast, within **1**·HBF_4 (81.6°), **1**·$2HBF_4$ (Ø 84.8°), and **2**·2MeCN (Ø 79.0°), the imidazole groups adopt a nearly orthogonal orientation. The N1–C2–N2 bond angles (**1**: 122.2°, **1**·HBF_4: 116.3°, **1**·$2HBF_4$: 116.1°, **2**·2MeCN: 116.5°) and the C2–N2–C3 angles (**1**: 130.3°, **1**·HBF_4: 126.2°, **1**·$2HBF_4$: 122.7°, **2**·2MeCN: 123.7°) are similar. The C–N bond distances (1.301 Å–1.340 Å) are within the range of typical C–N single and C=N double bonds.[108,109] In the solid state structure of **III**, the NHI groups are staggered in a similar fashion to **1** and rotated (Ø 53.8°) relative to the phenanthroline plane. A comparison of geometrical parameters is shown in Table 1.[63,110] Notably, the C_{phen}–N_{imine} and the endocyclic C_{NHI}–N_{NHI} bond lengths are shortened in **1** compared to **III**, while the N_{imine}=C_{NHI} bonds are elongated. This indicates a more pronounced π donation of the NHI groups towards the pyridine units in the case of **1**.

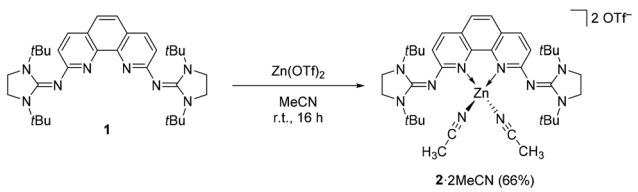

Scheme 2 Synthesis of the Zn^{II} complex **2**·2MeCN.

Electrochemical investigations

Considering the strong π-donor capability of the NHI groups,[7,55,63] we were curious to investigate their effect on the redox potentials and thus studied the electrochemical properties of **1**, **1**·$HB(C_6F_5)_4$, **2**·2MeCN and phen using cyclic voltammetry (CV) and differential pulse voltammetry (DPV) (see ESI† for details). For **1**, two partially reversible one-electron oxidation processes (−0.03 V and 0.38 V *vs.* Fc/Fc^+), one irreversible oxidation process (0.57 V *vs.* Fc/Fc^+) and two irreversible one-electron reductions at low potentials (−3.03 V and −3.18 V *vs.* Fc/Fc^+) are observed (Fig. 3a). The latter are significantly shifted cathodically when compared to phen (−2.63 V, −2.82 V *vs.* Fc/Fc^+) evidencing the increase of electron density within the aromatic system.[111] According to the DFT calculations, the HOMO and HOMO−1 of **1** are distributed over the phenanthroline moiety and imine N atoms and are mostly of π character (see Fig. S68 in the ESI†). Thus, the first two oxidation processes likely occur at the aromatic phenanthroline scaffold and the oxidation potential follows the same trend of

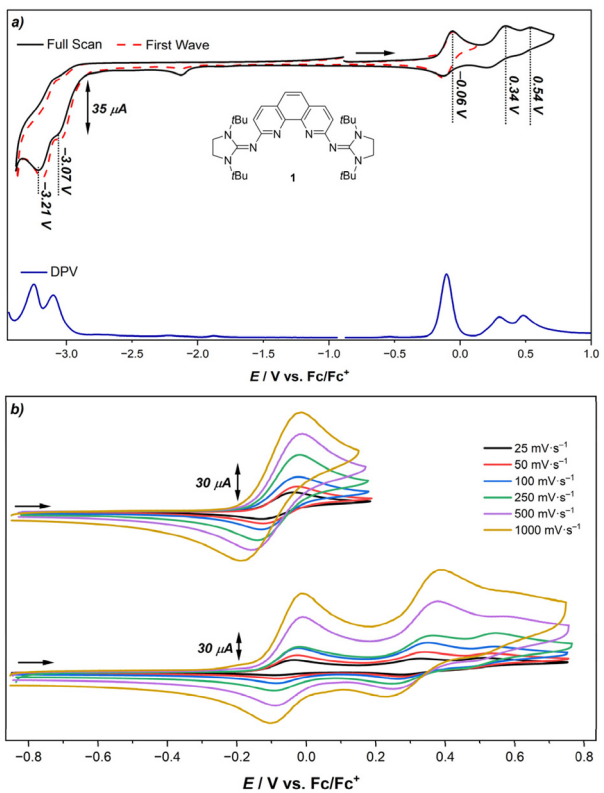

Fig. 3 (a) Cyclic voltammogram and differential pulse voltammogram of 1 under inert conditions. (CV: scan rate: 100 mV s^{-1}, in MeCN, electrolyte: [*n*-Bu_4N][PF_6] (0.1 M), working electrode: glassy carbon, counter electrode: Pt wire; DPV: step size: 5 mV, pulse time: 0.1 s, pulse size: 25 mV). Internally referenced against Fc^*/Fc^{*+} and reported against Fc/Fc^+. (b) Cyclic voltammogram of 1 under inert conditions at different potential windows and different scan rates (in MeCN, electrolyte: [*n*-Bu_4N][PF_6] (0.1 M), working electrode: glassy carbon, counter electrode: Pt wire). Internally referenced against Fc^*/Fc^{*+} and reported against Fc/Fc^+.

Table 2 First oxidation and first reduction potentials taken from the cyclic voltammograms measured at a scan rate of 100 mV s^{-1}. Potentials are reported against Fc/Fc^+ in MeCN

Compound	E^{red}_{1st}	E^{ox}_{1st}
Phen	−2.67 V	—
1	−3.07 V	−0.06 V
1·$HB(C_6F_5)_4$	−2.22 V	0.50 V
2·2MeCN	−2.64 V	0.71 V

the phenanthroline ligand in **III** (E^{ox}_{1st} = −0.26 V *vs.* Fc/Fc^+).[63] Similarly, the positive charges are stabilized through resonance structures which involve the NHI groups. However, due to the different substitution pattern, a third irreversible oxidation process is observed in the case of **1** (see Fig. S68 and S69 in the ESI† for details). Within the potential window of the first oxidation event, the process appears to be reversible even at low scan rates (Fig. 3b). Within the potential window including all oxidation events on the other hand, these processes only possess reversible character at higher scan rates. This indicates the formation of a short-lived species upon further oxidation.

In comparison to **1**, the protonated salt **1**·$HB(C_6F_5)_4$ is less electron-rich. Consistently, the first reduction potential is shifted anodically (E^{red}_{1st} = −2.19 V) and the first oxidation potential is shifted cathodically (E^{ox}_{1st} = 0.53 V). This trend was also observed in the CV studies of the zinc complex **2**·2MeCN (Table 2).

Photophysical properties

The photophysical properties of **1**, **1**·HBF4 and **2**·2MeCN were studied and compared with those of 1,10-phenanthroline (phen) for reference. Phen absorbs light in the UV region (200–320 nm) and displays a weak and short lived fluorescence emission ($\tau \leq 1$ ns, $\lambda_{em} \approx 360$ nm) at 298 K and a long lived phosphorescence (τ = 1.1 s, $\lambda_{em} \approx 460$ nm) at 77 K.[112–114] Protonation of phen induces a red-shift of the absorption and emission maxima.[69,102] This change of photophysical properties of phen and its derivatives in dependence of the pH or upon complexation to a metal center has led to their application as chemosensors.[66,115–118] **1** shows a complex photophysical behavior. As in phen, the luminescence of **1** at 77 K consists of both fluorescence and phosphorescence with dramatically different excited state lifetimes of nanoseconds and seconds, respectively. The short lifetime is consistent with rapid deactivation of the singlet excited state (S_1) *via* intersystem crossing (ISC) to the triplet excited sate (T_1). The T_1 in contrast is expected to have a very long-lived phosphorescence. Fig. 4 (A, top) shows the absorption spectra of **1** in THF at ambient temperature and at concentrations of 0.5, 1, 2, 3, 5, 10, 20, 30, 50, 100, and 200 μM. For **1**, the absorption at 290 nm is shifted to 280 nm in CH_2Cl_2. This band can be assigned to a spin-allowed $\pi \rightarrow \pi^*$ transition of the phenanthroline moiety of **1**.[113] Compared with unsubstituted 1,10-phenanthroline, where this band occurs at 264 nm in CH_2Cl_2, it is red shifted in **1**. This red shift indicates lowering of the π–π^* level due to the charge-transfer character resulting from the electron donation of the NHI groups into the phenanthroline π system. Therefore, the electron-donating properties of the substituents in **1** promote this red shift. This band at 290 nm shows no concentration dependence within the range 0.5 to 200 μM (Fig. 4A, above). By contrast, the second spin-allowed $\pi \rightarrow \pi^*$ transition in **1** exhibits a small red shift from 350 nm (0.5 μM) to 360 nm (200 μM). Since this transition is completely lacking in the UV/Vis spectrum of 1,10-phenanthroline,[113] it can be attributed to a shifted $\pi \rightarrow \pi^*$ band due to the imidazolidine substituents of **1**. In order to further characterise the individual UV/Vis excitations, TD-DFT calculations have been carried out. The resulting theoretical spectrum determined at B3LYP/6-31G(d,p) level in implicit dichloromethane was found in good agreement with the experimental reference (see Fig. S106, see in the ESI†). According to the calculations, three excitations giving rise to four dominant absorption bands at 361, 340, 301 and 299 nm are observed. Based on a visual inspection of the associated canonical molecular orbitals, all excitations can be classified to be predominantly $\pi \rightarrow \pi^*$ transitions. A linear dependence absorbance *versus* concentration is observed for **1** (Fig. S80†), following the Beer–Lambert law, indicating that aggregation is not occurring, even at the highest concentrations of 0.2 M. Fig. 4 (A, bottom) shows two main emission peaks at 464 and 550 nm when excited at 360 nm at ambient temperature. At the lowest concentrations, only the peak at 550 nm is present. At higher concentrations (5–200 μM), the emission is blue shifted to a maximum band at 464 nm. At low concentrations the lifetimes measured for the blue component (λ_{max} = 465 nm) has a short component of 0.9 ns (64%) and a longer-lived component of 8.0 ns (36%), while the longer wavelengths (λ_{em} = 550 nm) has a lifetime of 1.2 (28%) and 10.2 ns (72%) respectively. At higher concentrations, where the blue emission line dominates the spectrum, only a very long-lived emission decay is observed, on the order of 0.1 to 1.0 s. The concentration dependent photophysics is most likely the result of a triplet–triplet annihilation (TTA) process (Fig. 5). In the TTA process, two molecules in their triplet excited states diffuse together and form a molecule in the ground state (S_0) and one in the S_1 state ($T_1 + T_1 \rightarrow S_0 + S_1 \rightarrow 2S_0 + h\nu$). The lifetimes of the green and blue bands track the TTA rate, not the S_1 rate. The S_1 states formed by TTA decay by a combination of emission and ISC to the T_1, both of which are orders of magnitude faster than the TTA process that generated the S_1. The TTA process here is enabled by the long-lived T_1 state (τ = 0.1–1 s). Thus, at low concentration the optical density and thus the concentration of T_1 states formed on excitation is low and phosphorescence from T_1 outcompetes TTA. As the concentration is increased, the optical density increases leading to a higher T_1 concentration on excitation and TTA takes place leading to S_1 emission being the dominant process. Assuming the emission of **1** changes with concentration due to TTA, it is important to check that all emissions stem from the same excited states at all concentrations. The complete emission range from 420 to

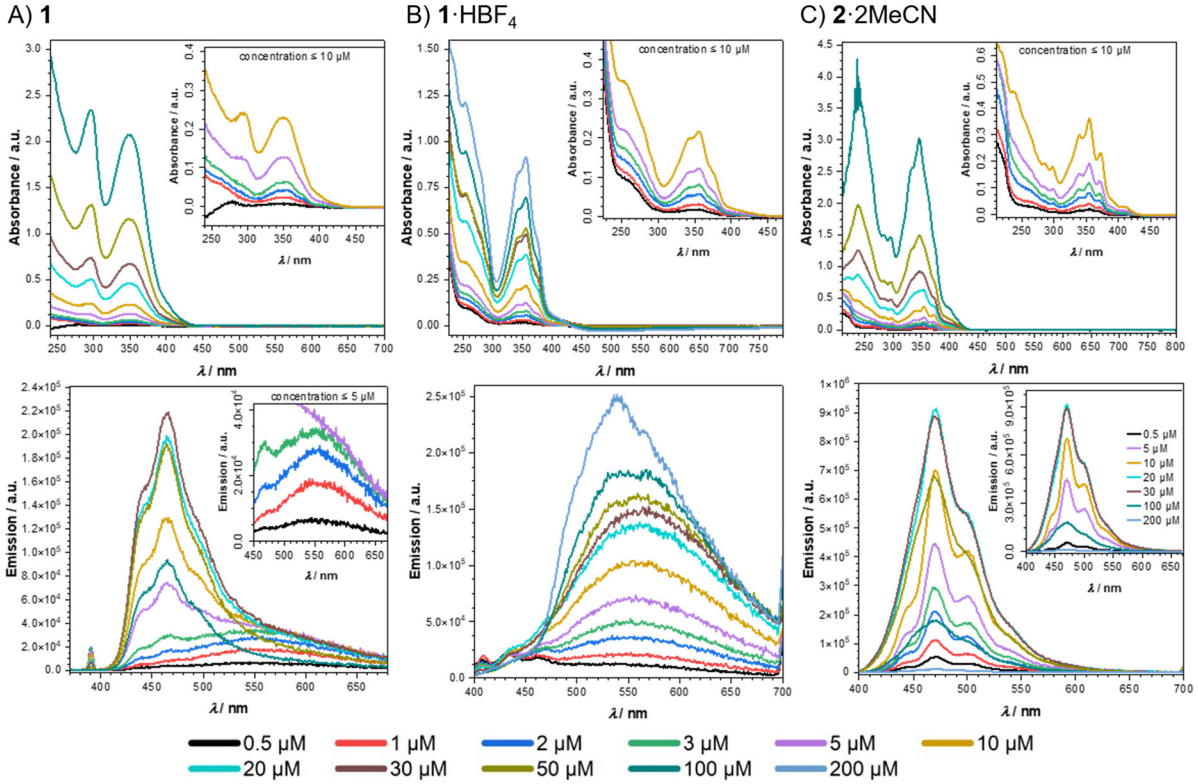

Fig. 4 The absorption and emission spectra of ligand **1** (A), **1**·HBF4 (B), and **2**·2MeCN (C) were measured in THF (A) and DMF (B and C), setting concentrations as 0.5, 1, 2, 3, 5, 10, 20, 30, 50, 100, and 200 μM. Emission spectra for an excitation at 360 nm (A) and 350 nm (B and C).

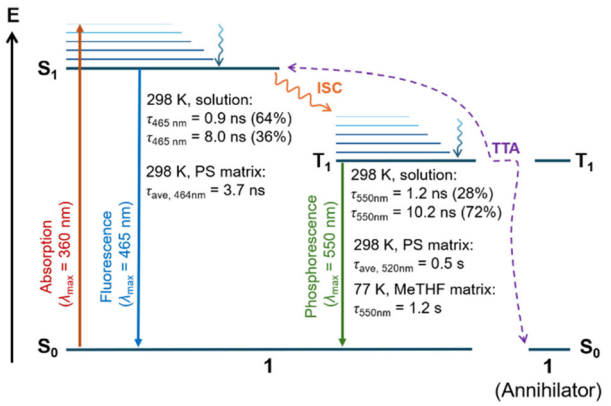

Fig. 5 Jablonski diagram of compound **1** including the intermolecular TTA process with a second molecule of **1** acting as annihilator (ISC = intersystem crossing, TTA = triplet–triplet annihilation, PS = polystyrene).

600 nm shows the same excitation peak at 360 nm (Fig. S77†), confirming that the same state formed on light absorption leads to both emission bands. These excitation peaks at 360 nm correspond to the $S_0 \rightarrow S_1$ absorption peak (Fig. 4A, top). To make the assignments of the excited states complete, the emissions of **1** in a polystyrene matrix at ambient temperature and in a 2-methyl-THF glass at 77 K were measured (Fig. 6 and Fig. S81†). At ambient temperature fluorescence appears (λ_{max} = 465 nm τ_{ave} = 3.7 ns), but the major contributor to the emission is the phosphorescence band at λ_{max} = 520 nm (τ_{ave} = 0.5 s). The emission band at 465 nm also shows a long time decay trace of 0.5 s, matching the value observed at 520 nm. At 77 K phosphorescence also plays a dominant role in the emission spectrum, differing from fluid solution at this concentration. This is typical for 1,10-phenanthroline and its derivatives.[113] The fluorescence at 77 K is centered at 450 nm, thus showing a typical rigidochromic effect on cooling,[119] when compared with the peak at 464 nm at ambient temperature in polystyrene.

The phosphorescence shows a similar rigidochromic effect, with λ_{max} at 513 nm with a shoulder at 540 nm at 77 K. This long-lived phosphorescence in the rigid matrix at 77 K is assigned to the lowest $^3\pi$–π^* level.[112,113,120] Its lifetime is independent of wavelength and for 450, 500, and 550 nm the same lifetimes of 1.2 s have been measured (see Fig. S79 in the ESI†) for an excitation wavelength of 360 nm. Note that in both polystyrene at ambient temperature and 2-methyl-THF at 77 K, diffusion is precluded, preventing TTA-based emission.

To further confirm these assignments, excited lifetime measurements were carried out. We measured the lifetimes of ligand **1** in air or degassed conditions at 0.5 and 100 μM for the peaks at 440, 464 and 550 nm (see Fig. S75 in the ESI†). The wavelength of excitation was 375 nm for all these measurements. At a given concentration (0.5 or 100 μM), the luminescence decay lifetimes at 440 and 464 nm are similar and are

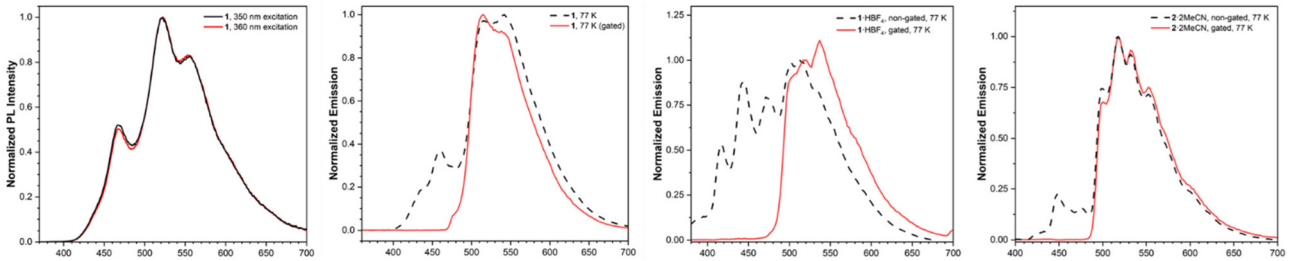

Fig. 6 Emission spectra of a polystyrene film of **1** (1% w/w) at ambient temperature (left) and 10 μM solution of **1**, **1**·HBF_4 and **2**·2MeCN recorded in glassy 2-methyl-THF at 77 K. The excitation wavelength was 360 nm. The dashed line contains both fluorescence and phosphorescence, whereas in the gated spectrum (red line) the fluorescence is suppressed. These spectra are independent on concentration.

not influenced markedly by O_2. In contrast, the lifetimes at 550 nm are longer for degassed samples, which is to be expected for the long-lived triplet state. Ligand **1** in low concentration (0.5 μM) showed a longer lifetime than the sample with the high concentration (100 μM), consistent with a faster TTA process at the high concentration (see the ESI† for details on the evaluation of the lifetimes).[121] The quantum yield of **1** in THF at ambient temperatures is 2%.

Substituted phenanthrolines show interesting photophysical properties, when coordinated to different metals.[122,123] Therefore, the photophysical properties of the protonated ligand **1**·HBF_4 and the Zn^{II} complex **2**·2MeCN were investigated. Fig. 4B shows that neither the absorption (top) nor the emission spectra (bottom) of **1**·HBF_4 show any indication of concentration dependence comparable to **1**. Plots of absorbance *versus* concentration for **1**·HBF_4 deviate from linearity at high concentrations, due to limited solubility in DMF, while the plot for the Zn^{II} complex **2**·2MeCN remains linear to the highest concentration (see Fig. S85 and S88†). Emission appears to come from phosphorescence only. Electrostatic repulsion of the cationic **1**·HBF_4 precludes TTA for this emitter. In contrast **2**·2MeCN (Fig. 4C) shows TTA-based emission, similar to that observed for **1** in THF, however, this complex does not show phosphorescence even at the lowest concentrations examined.

Both **1**·HBF_4 and the Zn^{II} complex **2**·2MeCN were further studied in glassy 2-methyl-THF at 77 K. The emission of **1**·HBF_4 and **2**·2MeCN at this temperature is dominated by phosphorescence (Fig. 6, two plots on the right). However, the lifetimes of **1**·HBF_4 are now dependent on wavelengths with biexponential decays with average lifetimes of 0.7 s at 500 nm and 0.5 s at 530 nm were determined for an excitation wavelength of 350 nm (see Fig. S84 in the ESI†). The lifetimes of **2**·2MeCN are longer, τ_{ave} = 1.3 to 1.9 s for 518 and 500 nm, respectively, for an excitation wavelength of 360 nm (see Fig. S87 in the ESI†). These long-lived $^3\pi\pi^*$ level[112,113,120] are typical for the phenanthroline moiety of **1**·HBF_4 and **2**·2MeCN. The quantum yield is higher for **1**·HBF_4 (10%) and **2**·2MeCN (4.0%) than for **1** (2.0%) in THF. The lifetimes of **1**·HBF_4 gives a biexponential decay at 450 nm of τ = 3.5 ns (68%) and 15.8 ns (32%), with a longer decay time of 31 ns observed at 500 and 550 nm (see Table S3 in the ESI†). The decay lifetime at 450 nm is largely due to ISC to T_1 and is slower than observed for **1**. The lifetimes of a 10 μM solution of **2**·2MeCN in degassed THF at 298 K are given in Table S4,† again showing very little dependence on the wavelengths of emission (τ_{ave} = 3.4 ns for the shorter components, see Table S4†).

Titration experiments were also carried out using HOTf as acid for the successive protonation or $Zn(OTf)_2$ for the complexation of **1**. Upon addition of 0.25–4.0 equivalents of acid, the spin-allowed $\pi \rightarrow \pi^*$ transition of the phenanthroline moiety at 250 nm in DMF increases, whereas the spin-allowed $\pi \rightarrow \pi^*$ transition at 350 nm decreases for the same amounts of HOTf (Fig. 7A, above). A comparable increased luminescence during the addition of acid was observed for 2,3,7,8-tetrakis(tetramethylguanidino)-phenazine.[38]

Upon excitation at 350 nm, the emission at 550 nm increases for added HOTf in the range of 0.25–1.5 equivalents (Fig. 7A, below). In contrast, addition of more than 2.0 equivalents of HOTf hampers the luminescence intensity (Fig. 7A below).

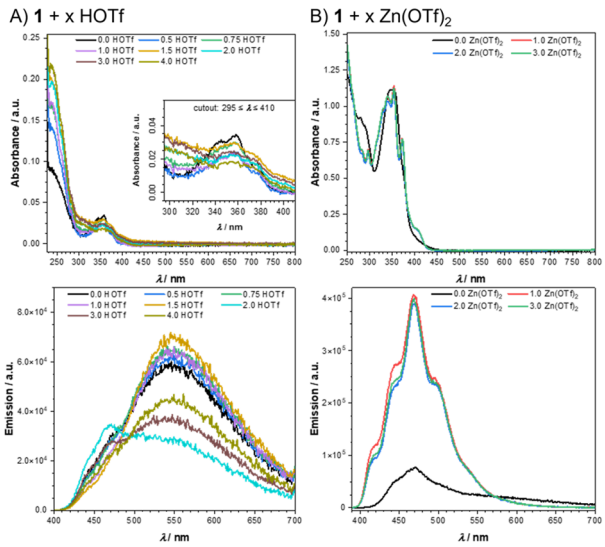

Fig. 7 (A) UV/Vis (above) and emission (below, excitation at 350 nm) spectra of **1** in DMF, depending on the addition of HOTf (0.5–4.0 equivalents); (B) UV/Vis (above) and emission (below, excitation at 350 nm) spectra of **1** in DMF, depending on the addition of Zn(OTf)2 (1.0–3.0 equivalents).

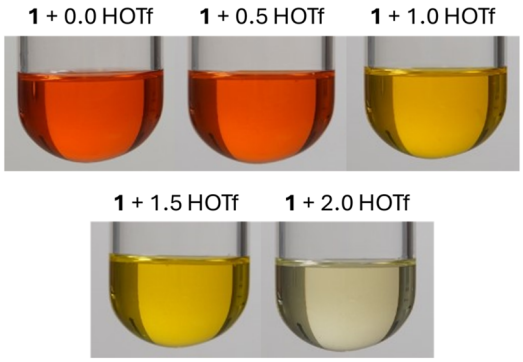

Fig. 8 Images of 0.15 M solution of 1 in DCM after successive addition of HOTf under inert conditions.

Fig. 7B shows that a luminescence enhancement could also be achieved by complexation of **1** with Zn^{II}.

This is a typical example of structure-driven photoluminescence enhancement by Zn^{II}.[66,124,125] In the case of **1** after addition of one equivalent Zn^{II} no further increase of luminescence could be observed (Fig. 7B, below). Thus, this effect corresponds to the formation of **2**·2MeCN (see Fig. 2), where coordination experiments have shown that no further uptake of Zn^{II} by **2**·2MeCN is possible. In a similar vein to the titration experiments, the color change of a DCM solution of **1** upon successive protonation was investigated under inert conditions (Fig. 8). The initially orange solution of **1** gradually turns yellow (1.0 equivalents of HOTf) matching the color of the isolated **1**·HBF_4 and then fades upon addition of more acid (≤2.0 equivalents), also matching the off-white to pale-yellow color of the isolated **1**·$2HBF_4$. Further addition of HOTf under inert conditions (>2.0 equivalents) causes the solution to become slightly yellow and ultimately turbid (see Fig. S92 in the ESI†). This indicates that protonation beyond $[\mathbf{1}\cdot 2H]^{2+}$ is potentially feasible in a non-coordinating solvent using excess HOTf.

Conclusions

In conclusion, we present the synthesis and characterization of a new electron-rich 1,10-phenanthroline ligand, **1**, bearing bulky NHI groups adjacent to the coordination center. Electrochemical studies of **1** are in line with previously reported guanidyl-substituted polypyridine ligands and confirm the increased electron density of the ligand due to the π-donation of the NHI substituents. Coordination experiments with Zn^{II} showed that **1** binds a single metal center, coordinating selectively at the phenanthroline N atoms, which is in contrast to the Janus head pro-type ligand **III** and the preference of **I** to coordinate with the guanidyl N atoms. Likewise, the protonation of **1** was theoretically and experimentally confirmed to take place at one of the phenanthroline N atoms. The second protonation, however, is less regioselective, leading to tautomeric forms in solution, with DFT calculations indicating a 12.6 kJ mol^{-1} energetic preference for protonation at the imine nitrogen atom. Photophysical experiments show that the optical properties of **1** are highly sensitive to protonation, concentration, and metal coordination. Upon protonation at the phenanthroline nitrogen atoms, the emission intensity increases, but it decreases upon binding of a second proton, presumably due to protonation of an imine group.[38] The UV/Vis absorption at 350 nm, responsible for the red-to-orange color of **1**, fades upon protonation, corresponding to a visible color change. In addition, the absorption and emission of **1** are dependent on concentration due to TTA in solution. This effect is absent in the cases of the ionic compounds **1**·HBF_4 and **2**·2MeCN. Furthermore, coordination with Zn^{II} significantly enhances emission, as steric constraints lead to rigidification of the ligand scaffold.

In summary, **1** is an electron-rich ligand with four donor sites positioned within a coordination cavity shaped by bulky *tert*-butyl groups. Due to the strong π-donating effect of the NHI groups, the phenanthroline nitrogen atoms exhibit significantly enhanced basicity (pK_{BH^+} (ACN) = 25.0) driving preferential coordination of Lewis acids *via* the phenanthroline core. This electronic effect also significantly impacts the ligand's redox and optical properties. Ongoing studies in our group are focused on further exploring its coordination chemistry and multiple-site binding capabilities.

Author contributions

J. H. F. carried out the experiments and synthesized and characterized the new compounds. L. F. B. W. and J. H. F. developed the synthesis of **1**. F. D. directed the investigation. Investigations on the optical properties were performed by X. Z., A. A., K. B., A. M. and P. B. Electrochemical measurements were made by K. B. and A. M. DFT calculations were performed by T. S. H. SCXRD studies were carried out by M. S. The manuscript was written by J. H. F., P. B. and F. D., and edited by F. D., K. B., A. M., M. T. and L. D. C. All authors have given approval for the final version of the manuscript.

Conflicts of interest

There are no conflicts to declare.

Data availability

The data supporting this article have been included as part of the ESI.†

Acknowledgements

We sincerely thank the Tiroler Wissenschaftsförderung (TWF, F.45075) for funding to realize this project and the German Academic Scholarship Foundation for a PhD fellowship (L. F. B. W.).

References

1 N. Kuhn, R. Fawzi, M. Steimann, J. Wiethoff, D. Bläser and R. Boese, Synthese und Struktur von 2-Imino-1,3-dimethylimidazolin/Synthesis and Structure of 2-Imino-1,3-dimethylimidazoline, *Z. Naturforsch., B*, 1995, **50**, 1779–1784.

2 N. Kuhn, R. Fawzi, M. Steimann, J. Wiethoff and G. Henkel, Synthese und Struktur von [ImNCS 2 K] (ImN = 1,3-Dimethylimidazolin-2-imino): ein neuartiges Kaliumdithiocarbiminat, *Z. Anorg. Allg. Chem.*, 1997, **623**, 1577–1582.

3 N. Kuhn, M. Göhner, M. Grathwohl, J. Wiethoff, G. Frenking and Y. Chen, 2-Iminoimidazoline—starke Stickstoffbasen als Koordinationspartner in der Anorganischen Chemie, *Z. Anorg. Allg. Chem.*, 2003, **629**, 793–802.

4 N. Kuhn, R. Fawzi, M. Steimann and J. Wiethoff, Derivate des Imidazols. XXIII. 2-Iminoimidazolin-Derivate des Magnesiums und Aluminiums, *Z. Anorg. Allg. Chem.*, 1997, **623**, 554–560.

5 N. Kuhn, U. Abram, C. Maichle-Mößmer and J. Wiethoff, Derivate des Imidazols. XXIV [1]. $[Li_{12}O_2Cl_2(ImN)_8(THF)4]\cdot 8THF$: Ein Peroxo–Komplex des Lithiums mit neuartiger Käfigstruktur, *Z. Anorg. Allg. Chem.*, 1997, **623**, 1121–1124.

6 A. Doddi, M. Peters and M. Tamm, N-Heterocyclic, Carbene Adducts of Main Group Elements and Their Use as Ligands in Transition Metal Chemistry, *Chem. Rev.*, 2019, **119**, 6994–7112.

7 X. Wu and M. Tamm, Transition metal complexes supported by highly basic imidazolin-2-iminato and imidazolin-2-imine N-donor ligands, *Coord. Chem. Rev.*, 2014, **260**, 116–138.

8 T. Ochiai, D. Franz and S. Inoue, Applications of N-heterocyclic imines in main group chemistry, *Chem. Soc. Rev.*, 2016, **45**, 6327–6344.

9 A. G. Trambitas, T. K. Panda and M. Tamm, Rare Earth Metal Complexes Supported by Ancillary Imidazolin-2-iminato Ligands, *Z. Anorg. Allg. Chem.*, 2010, **636**, 2156–2171.

10 M. Tamm, S. Randoll, T. Bannenberg and E. Herdtweck, Titanium complexes with imidazolin-2-iminato ligands, *Chem, Commun.*, 2004, 876–877.

11 F. Dielmann, O. Back, M. Henry-Ellinger, P. Jerabek, G. Frenking and G. Bertrand, A crystalline singlet phosphinonitrene: a nitrogen atom-transfer agent, *Science*, 2012, **337**, 1526–1528.

12 F. Dielmann, C. E. Moore, A. L. Rheingold and G. Bertrand, Crystalline, Lewis base-free, cationic phosphoranimines (iminophosphonium salts), *J. Am. Chem. Soc.*, 2013, **135**, 14071–14073.

13 P. Mehlmann, T. Witteler, L. F. B. Wilm and F. Dielmann, Isolation, characterization and reactivity of three-coordinate phosphorus dications isoelectronic to alanes and silylium cations, *Nat. Chem.*, 2019, **11**, 1139–1143.

14 M. A. Wünsche, T. Witteler and F. Dielmann, Lewis Base Free Oxophosphonium Ions: Tunable, Trigonal-Planar Lewis Acids, *Angew. Chem., Int. Ed.*, 2018, **57**, 7234–7239.

15 P. Löwe, T. Witteler and F. Dielmann, Lewis base-free thiophosphonium ion: a cationic sulfur atom transfer reagent, *Chem. Commun.*, 2021, **57**, 5043–5046.

16 P. Löwe, M. A. Wünsche, F. R. S. Purtscher, J. Gamper, T. S. Hofer, L. F. B. Wilm, M. B. Röthel and F. Dielmann, Terminal methylene phosphonium ions: precursors for transient monosubstituted phosphinocarbenes, *Chem. Sci.*, 2023, **14**, 7928–7935.

17 D. Wendel, T. Szilvási, C. Jandl, S. Inoue and B. Rieger, Twist of a Silicon-Silicon Double Bond: Selective Anti-Addition of Hydrogen to an Iminodisilene, *J. Am. Chem. Soc.*, 2017, **139**, 9156–9159.

18 D. Wendel, D. Reiter, A. Porzelt, P. J. Altmann, S. Inoue and B. Rieger, Silicon and Oxygen's Bond of Affection: An Acyclic Three-Coordinate Silanone and Its Transformation to an Iminosiloxysilylene, *J. Am. Chem. Soc.*, 2017, **139**, 17193–17198.

19 F. S. Tschernuth, F. Hanusch, T. Szilvási and S. Inoue, Isolation and Reactivity of Chlorotetryliumylidenes Using a Bidentate Bis(N-heterocyclic imine) Ligand, *Organometallics*, 2020, **39**, 4265–4272.

20 S. V. Hirmer, F. S. Tschernuth, F. Hanusch, R. Baierl, M. Muhr and S. Inoue, Modification of bidentate bis(N-heterocyclic imine) ligands for low-valent main group complexes, *Mendeleev Commun.*, 2022, **32**, 16–18.

21 D. Franz, E. Irran and S. Inoue, Isolation of a three-coordinate boron cation with a boron-sulfur double bond, *Angew. Chem., Int. Ed.*, 2014, **53**, 14264–14268.

22 M. W. Lui, C. Merten, M. J. Ferguson, R. McDonald, Y. Xu and E. Rivard, Contrasting reactivities of silicon and germanium complexes supported by an N-heterocyclic guanidine ligand, *Inorg. Chem.*, 2015, **54**, 2040–2049.

23 R. F. Weitkamp, B. Neumann, H.-G. Stammler and B. Hoge, Phosphorus-Containing Superbases: Recent Progress in the Chemistry of Electron-Abundant Phosphines and Phosphazenes, *Chem. – Eur. J.*, 2021, **27**, 10807–10825.

24 F. Buß, M. B. Röthel, J. A. Werra, P. Rotering, L. F. B. Wilm, C. G. Daniliuc, P. Löwe and F. Dielmann, Tris(tetramethylguanidinyl)phosphine: The Simplest Non-ionic Phosphorus Superbase and Strongly Donating Phosphine Ligand, *Chem. – Eur. J.*, 2022, **28**, e202104021.

25 M. A. Wünsche, P. Mehlmann, T. Witteler, F. Buß, P. Rathmann and F. Dielmann, Imidazolin-2-ylidenaminophosphines as Highly Electron-Rich Ligands for Transition-Metal Catalysts, *Angew. Chem., Int. Ed.*, 2015, **54**, 11857–11860.

26 P. Mehlmann, C. Mück-Lichtenfeld, T. T. Y. Tan and F. Dielmann, Tris(imidazolin-2-ylidenamino)phosphine: A Crystalline Phosphorus(III) Superbase That Splits Carbon Dioxide, *Chem. – Eur. J.*, 2017, **23**, 5929–5933.

27 P. Rotering, L. F. B. Wilm, J. A. Werra and F. Dielmann, Pyridinylidenaminophosphines: Facile Access to Highly Electron-Rich Phosphines, *Chem. – Eur. J.*, 2020, **26**, 406–411.
28 M. Abdinejad, L. F. B. Wilm, F. Dielmann and H. B. Kraatz, Electroreduction of CO2 Catalyzed by Nickel Imidazolin-2-ylidenamino-Porphyrins in Both Heterogeneous and Homogeneous Molecular Systems, *ACS Sustainable Chem. Eng.*, 2021, **9**, 521–530.
29 J. A. Murphy, Discovery and development of organic super-electron-donors, *J. Org. Chem.*, 2014, **79**, 3731–3746.
30 J. A. Murphy, J. Garnier, S. R. Park, F. Schoenebeck, S. Zhou and A. T. Turner, Super-electron donors: bis-pyridinylidene formation by base treatment of pyridinium salts, *Org. Lett.*, 2008, **10**, 1227–1230.
31 S. S. Hanson, N. A. Richard and C. A. Dyker, Powerful Bispyridinylidene Organic Reducing Agents with Iminophosphorano π-Donor Substituents, *Chem. – Eur. J.*, 2015, **21**, 8052–8055.
32 S. S. Hanson, E. Doni, K. T. Traboulsee, G. Coulthard, J. A. Murphy and C. A. Dyker, Pushing the limits of neutral organic electron donors: a tetra(iminophosphorano)-substituted bispyridinylidene, *Angew. Chem., Int. Ed.*, 2015, **54**, 11236–11239.
33 B. Eberle, E. Kaifer and H.-J. Himmel, A Stable Hexakis (guanidino)benzene: Realization of the Strongest Neutral Organic Four-Electron Donor, *Angew. Chem., Int. Ed.*, 2017, **56**, 3360–3363.
34 M. M. Burgoyne, T. M. MacDougall, Z. N. Haines, J. W. Conrad, L. A. Calhoun, A. Decken and C. A. Dyker, A strong organic electron donor incorporating highly π-donating triphenylphosphonium ylidyl substituents, *Org. Biomol. Chem.*, 2019, **17**, 9726–9733.
35 P. W. Antoni, C. Golz and M. M. Hansmann, Organic Four-Electron Redox Systems Based on Bipyridine and Phenanthroline Carbene Architectures, *Angew. Chem., Int. Ed.*, 2022, **61**, e202203064.
36 J. Garnier, A. R. Kennedy, L. E. A. Berlouis, A. T. Turner and J. A. Murphy, Structure and reactivity in neutral organic electron donors derived from 4-dimethylaminopyridine, *Beilstein J. Org. Chem.*, 2010, **6**, DOI: 10.3762/bjoc.6.73.
37 J. Broggi, T. Terme and P. Vanelle, Organic electron donors as powerful single-electron reducing agents in organic synthesis, *Angew. Chem., Int. Ed.*, 2014, **53**, 384–413.
38 E. Bindewald, R. Lorenz, O. Hübner, D. Brox, D.-P. Herten, E. Kaifer and H.-J. Himmel, Tetraguanidino-functionalized phenazine and fluorene dyes: synthesis, optical properties and metal coordination, *Dalton Trans.*, 2015, **44**, 3467–3485.
39 R. Lorenz, E. Kaifer, H. Wadepohl and H.-J. Himmel, Di- and tetranuclear transition metal complexes of a tetrakisguanidino-substituted phenazine dye by stepwise coordination, *Dalton Trans.*, 2018, **47**, 11016–11029.
40 J. Osterbrink, F. Dos Santos, E. Kaifer and H.-J. Himmel, Redox Reactivity Control Through Electromerism, *Eur. J. Inorg. Chem.*, 2024, **27**, e202400070.
41 A. Maronna, O. Hübner, M. Enders, E. Kaifer and H.-J. Himmel, Bisguanidines with biphenyl, binaphthyl, and bipyridyl cores: proton-sponge properties and coordination chemistry, *Chem. – Eur. J.*, 2013, **19**, 8958–8977.
42 P. Roquette, A. Maronna, A. Peters, E. Kaifer, H.-J. Himmel, C. Hauf, V. Herz, E.-W. Scheidt and W. Scherer, On the electronic structure of Ni(II) complexes that feature chelating bisguanidine ligands, *Chem. – Eur. J.*, 2010, **16**, 1336–1350.
43 S. Wiesner, A. Wagner, O. Hübner, E. Kaifer and H.-J. Himmel, Thermochromism of Cu(I) Tetrakisguanidine Complexes: Reversible Activation of Metal-to-Ligand Charge-Transfer Bands, *Chem. – Eur. J.*, 2015, **21**, 16494–16503.
44 Y. Wei, G. N. Sastry and H. Zipse, Methyl cation affinities of commonly used organocatalysts, *J. Am. Chem. Soc.*, 2008, **130**, 3473–3477.
45 C. Lindner, R. Tandon, B. Maryasin, E. Larionov and H. Zipse, Cation affinity numbers of Lewis bases, *Beilstein J. Org. Chem.*, 2012, **8**, 1406–1442.
46 P. Hommes, C. Fischer, C. Lindner, H. Zipse and H.-U. Reissig, Unprecedented strong Lewis bases–synthesis and methyl cation affinities of dimethylamino-substituted terpyridines, *Angew. Chem., Int. Ed.*, 2014, **53**, 7647–7651.
47 I. Despotović and R. Vianello, Engineering exceptionally strong oxygen superbases with 1,8-diazanaphthalene di-N-oxides, *Chem. Commun.*, 2014, **50**, 10941–10944.
48 C. H. Suresh and S. R. Gadre, A Novel Electrostatic Approach to Substituent Constants: Doubly Substituted Benzenes, *J. Am. Chem. Soc.*, 1998, **120**, 7049–7055, (*J. Am. Chem. Soc.*, 1998, **120**, 10276).
49 F. B. Sayyed and C. H. Suresh, An electrostatic scale of substituent resonance effect, *Tetrahedron Lett.*, 2009, **50**, 7351–7354.
50 G. S. Remya and C. H. Suresh, Quantification and classification of substituent effects in organic chemistry: a theoretical molecular electrostatic potential study, *Phys. Chem. Chem. Phys.*, 2016, **18**, 20615–20626.
51 V. U. Krishnapriya and C. H. Suresh, Imidazolin-2-imine and Imidazolin-2-methylidene Substitutions to Benzene, Pyridine, Phosphine, and N -Heterocyclic Carbene Predict Highly Electron-rich Ligands, *Organometallics*, 2023, **42**, 571–580.
52 Y. Han, H. V. Huynh and G. K. Tan, Syntheses and Characterizations of Pd(II) Complexes Incorporating a N -Heterocyclic Carbene and Aromatic N -Heterocycles, *Organometallics*, 2007, **26**, 6447–6452.
53 H. V. Huynh, Y. Han, R. Jothibasu and J. An Yang, ^{13}C NMR Spectroscopic Determination of Ligand Donor Strengths Using N-Heterocyclic Carbene Complexes of Palladium(II), *Organometallics*, 2009, **28**, 5395–5404.

54 Q. Teng and H. V. Huynh, A unified ligand electronic parameter based on ^{13}C NMR spectroscopy of N-heterocyclic carbene complexes, *Dalton Trans.*, 2017, **46**, 614–627.

55 J. H. Franzen, L. F. B. Wilm, P. Rotering, K. Wurst, M. Seidl and F. Dielmann, Electron-rich pyridines with para-N-heterocyclic imine substituents: ligand properties and coordination to CO_2, SO_2, BCl_3 and PdII complexes, *Dalton Trans.*, 2024, **53**, 11876–11883.

56 J. L. Doran, B. Hon and K. R. Leopold, Rotational spectrum and structure of the pyridine–CO_2 van der Waals complex, *J. Mol. Struct.*, 2012, **1019**, 191–195.

57 K. D. Vogiatzis, A. Mavrandonakis, W. Klopper and G. E. Froudakis, Ab initio study of the interactions between CO(2) and N-containing organic heterocycles, *ChemPhysChem*, 2009, **10**, 374–383.

58 J. W. Keller, Sulfur Dioxide-Pyridine Dimer. FTIR and Theoretical Evidence for a Low-Symmetry Structure, *J. Phys. Chem. A*, 2015, **119**, 10390–10398.

59 H.-J. Himmel, Guanidinyl–Functionalized Aromatic Compounds (GFAs) – Charge and Spin Density Studies as Starting Points for the Development of a New Class of Redox–active Ligands, *Z. Anorg. Allg. Chem.*, 2013, **639**, 1940–1952.

60 S. Stang, A. Lebkücher, P. Walter, E. Kaifer and H.-J. Himmel, Redox–Active Guanidine Ligands with Pyridine and p –Benzoquinone Backbones, *Eur. J. Inorg. Chem.*, 2012, **2012**, 4833–4845.

61 L. Lohmeyer, E. Kaifer, H. Wadepohl and H.-J. Himmel, 1,2,5,6-Tetrakis(guanidino)-Naphthalenes: Electron Donors, Fluorescent Probes and Redox-Active Ligands, *Chem. – Eur. J.*, 2020, **26**, 5834–5845.

62 F. T. Edelmann, Recent Progress in the Chemistry of Metal Amidinates and Guanidinates, *Adv. Organomet. Chem.*, 2013, **61**, 55–374.

63 J. Ortmeyer, Y. Vukadinovic, A. Neuba, H. Egold, U. Flörke and G. Henkel, Combining a Phenanthroline Moiety with Two Peralkylated Guanidine Residues: Janus Head Pro-Ligands, *Eur. J. Org. Chem.*, 2017, 6085–6095.

64 J. Ortmeyer, Y. Vukadinovic, A. Neuba, U. Flörke and G. Henkel, Combining a Phenanthroline Moiety with Peralkylated Guanidine Residues: Homometallic Cu II , Ni II and Zn II Halide Complexes with Site-Differentiating Janus Head Ligands, *Eur. J. Inorg. Chem.*, 2018, **2018**, 5176–5190.

65 C. Queffélec, P. B. Pati and Y. Pellegrin, Fifty Shades of Phenanthroline: Synthesis Strategies to Functionalize 1,10-Phenanthroline in All Positions, *Chem. Rev.*, 2024, **124**, 6700–6902.

66 P. Alreja and N. Kaur, Recent advances in 1,10-phenanthroline ligands for chemosensing of cations and anions, *RSC Adv.*, 2016, **6**, 23169–23217.

67 P. G. Sammes and G. Yahioglu, 1,10-Phenanthroline: a versatile ligand, *Chem. Soc. Rev.*, 1994, **23**, 327.

68 W. W. Brandt, F. P. Dwyer and E. D. Gyarfas, Chelate Complexes of 1,10-Phenanthroline and Related Compounds, *Chem. Rev.*, 1954, **54**, 959–1017.

69 G. Accorsi, A. Listorti, K. Yoosaf and N. Armaroli, 1,10-phenanthrolines: versatile building blocks for luminescent molecules, materials and metal complexes, *Chem. Soc. Rev.*, 2009, **38**, 1690–1700.

70 Z. Ge, T. Hayakawa, S. Ando, M. Ueda, T. Akiike, H. Miyamoto, T. Kajita and M. Kakimoto, Novel bipolar bathophenanthroline containing hosts for highly efficient phosphorescent OLEDs, *Org. Lett.*, 2008, **10**, 421–424.

71 Y. Tao, C. Yang and J. Qin, Organic host materials for phosphorescent organic light-emitting diodes, *Chem. Soc. Rev.*, 2011, **40**, 2943–2970.

72 A. Buyruk, D. Blätte, M. Günther, M. A. Scheel, N. F. Hartmann, M. Döblinger, A. Weis, A. Hartschuh, P. Müller-Buschbaum, T. Bein and T. Ameri, 1,10-Phenanthroline as an Efficient Bifunctional Passivating Agent for MAPbI3 Perovskite Solar Cells, *ACS Appl. Mater. Interfaces*, 2021, **13**, 32894–32905.

73 N. Kandasamy, N. Keerthi and J. Jeyasekaran, Mixed Ligand Copper(I) Complexes as Emitters Enable Higher OLED Device Performance for Energy-Harvesting Applications, *ACS Appl. Electron. Mater.*, 2023, **5**, 4805–4815.

74 B. E. Halcrow and W. O. Kermack, Attempts to find new antimalarials; derivatives of o-phenanthroline (7:8:3′:2′-pyridoquinoline), *J. Chem. Soc.*, 1946, 155–157.

75 M. A. de Zwart, H. M. Bastiaans, H. van der Goot and H. Timmerman, Synthesis and copper-dependent antimycoplasmal activity of amides and amidines derived from 2-amino-1,10-phenanthroline, *J. Med. Chem.*, 1991, **34**, 1193–1201.

76 S. L. H. Higgins and K. J. Brewer, Designing red-light-activated multifunctional agents for the photodynamic therapy, *Angew. Chem., Int. Ed.*, 2012, **51**, 11420–11422.

77 N. M. Gueddouda, M. R. Hurtado, S. Moreau, L. Ronga, R. N. Das, S. Savrimoutou, S. Rubio, A. Marchand, O. Mendoza, M. Marchivie, L. Elmi, A. Chansavang, V. Desplat, V. Gabelica, A. Bourdoncle, J.-L. Mergny and J. Guillon, Design, Synthesis, and Evaluation of 2,9-Bis (substituted-aminomethyl)phenyl-1,10-phenanthroline Derivatives as G-Quadruplex Ligands, *ChemMedChem*, 2017, **12**, 146–160.

78 A. Nano, J. Dai, J. M. Bailis and J. K. Barton, Rhodium Complexes Targeting DNA Mismatches as a Basis for New Therapeutics in Cancers Deficient in Mismatch Repair, *Biochemistry*, 2021, **60**, 2055–2063.

79 J. Guillon, A. Cohen, C. Boudot, S. Monic, S. Savrimoutou, S. Moreau, S. Albenque-Rubio, C. Lafon-Schmaltz, A. Dassonville-Klimpt, J.-L. Mergny, L. Ronga, M. Bernabeu de Maria, J. Lamarche, C. D. Lago, E. Largy, V. Gabelica, S. Moukha, P. Dozolme, P. Agnamey, N. Azas, C. Mullié, B. Courtioux and P. Sonnet, Design, Synthesis, and Antiprotozoal Evaluation of New Promising 2,9-Bis(substituted-aminomethyl)-4,7-phenyl-1,10-phenanthroline Derivatives, a Potential Alternative Scaffold to Drug Efflux, *Pathogens*, 2022, **11**, 1339.

80 F. C. Rix, M. Brookhart and P. S. White, Mechanistic Studies of the Palladium(II)-Catalyzed Copolymerization of

Ethylene with Carbon Monoxide, *J. Am. Chem. Soc.*, 1996, **118**, 4746–4764.

81 J. E. McGarrah, Y. J. Kim, M. Hissler and R. Eisenberg, Toward a molecular photochemical device: a triad for photoinduced charge separation based on a platinum diimine bis(acetylide) chromophore, *Inorg. Chem.*, 2001, **40**, 4510–4511.

82 Y. Himeda, N. Onozawa-Komatsuzaki, H. Sugihara and K. Kasuga, Simultaneous Tuning of Activity and Water Solubility of Complex Catalysts by Acid-Base Equilibrium of Ligands for Conversion of Carbon Dioxide, *Organometallics*, 2007, **26**, 702–712.

83 M. G. Pfeffer, B. Schäfer, G. Smolentsev, J. Uhlig, E. Nazarenko, J. Guthmuller, C. Kuhnt, M. Wächtler, B. Dietzek, V. Sundström and S. Rau, Palladium versus platinum: the metal in the catalytic center of a molecular photocatalyst determines the mechanism of the hydrogen production with visible light, *Angew. Chem., Int. Ed.*, 2015, **54**, 5044–5048.

84 S. Rau, B. Schäfer, D. Gleich, E. Anders, M. Rudolph, M. Friedrich, H. Görls, W. Henry and J. G. Vos, A supramolecular photocatalyst for the production of hydrogen and the selective hydrogenation of tolane, *Angew. Chem., Int. Ed.*, 2006, **45**, 6215–6218.

85 L. Jiao, E. Herdtweck and T. Bach, Pd(II)-catalyzed regioselective 2-alkylation of indoles via a norbornene-mediated C-H activation: mechanism and applications, *J. Am. Chem. Soc.*, 2012, **134**, 14563–14572.

86 T. Moragas, M. Gaydou and R. Martin, Nickel-Catalyzed Carboxylation of Benzylic C-N Bonds with CO2, *Angew. Chem., Int. Ed.*, 2016, **55**, 5053–5057.

87 B. Guan, J. Liu, J. Leng, T. Fan and L. Tong, Hydrogen Evolution Catalysis by Cobalt Complexes of an Aza-bridged Bis-1,10-phenanthroline Ligand Bearing Pendant Basic Sites, *ChemCatChem*, 2024, **16**, e202401284.

88 A. Bencini and V. Lippolis, 1,10-Phenanthroline: A versatile building block for the construction of ligands for various purposes, *Coord. Chem. Rev.*, 2010, **254**, 2096–2180.

89 A. Juris, V. Balzani, F. Barigelletti, S. Campagna, P. Belser and A. von Zelewsky, Ru(II) polypyridine complexes: photophysics, photochemistry, eletrochemistry, and chemiluminescence, *Coord. Chem. Rev.*, 1988, **84**, 85–277.

90 A. J. Lees, *Photophysics of Organometallics*, Topics in Organometallic Chemistry 29, Springer: Berlin, Heidelberg, 2010, **https://ebookcentral.proquest.com/lib/kxp/detail.action?docID=3064880**.

91 S. Quici, M. Cavazzini, G. Marzanni, G. Accorsi, N. Armaroli, B. Ventura and F. Barigelletti, Visible and near-infrared intense luminescence from water-soluble lanthanide Tb(III), Eu(III), Sm(III), Dy(III), Pr(III), Ho(III), Yb(III), Nd(III), Er(III) complexes, *Inorg. Chem.*, 2005, **44**, 529–537.

92 S. Quici, C. Scalera, M. Cavazzini, G. Accorsi, M. Bolognesi, L. Armelao and G. Bottaro, Highly Photoluminescent Silica Layers Doped with Efficient Eu (III) and Tb(III) Antenna Complexes, *Chem. Mater.*, 2009, **21**, 2941–2949.

93 J. Beaudelot, S. Oger, S. Peruško, T.-A. Phan, T. Teunens, C. Moucheron and G. Evano, Photoactive Copper Complexes: Properties and Applications, *Chem. Rev.*, 2022, **122**, 16365–16609.

94 V. Balzani, *Photochemistry and Photophysics of Coordination Compounds I*, Topics in Current Chemistry Ser v.280, Springer, Berlin, *2007 edn*, 2007, **https://ebookcentral.proquest.com/lib/kxp/detail.action?docID=7201737**.

95 Y. Zhang, M. Schulz, M. Wächtler, M. Karnahl and B. Dietzek, Heteroleptic diimine–diphosphine Cu(I) complexes as an alternative towards noble-metal based photosensitizers: Design strategies, photophysical properties and perspective applications, *Coord. Chem. Rev.*, 2018, **356**, 127–146.

96 R. A. Kunetskiy, S. M. Polyakova, J. Vavřík, I. Císařová, J. Saame, E. R. Nerut, I. Koppel, I. A. Koppel, A. Kütt, I. Leito and I. M. Lyapkalo, A new class of organosuperbases, N-alkyl- and N-aryl-1,3-dialkyl-4,5-dimethylimidazol-2-ylidene amines: synthesis, structure, pK(BH+) measurements, and properties, *Chem. – Eur. J.*, 2012, **18**, 3621–3630.

97 L. F. B. Wilm, T. Eder, C. Mück-Lichtenfeld, P. Mehlmann, M. Wünsche, F. Buß and F. Dielmann, Reversible CO2 fixation by N-heterocyclic imines forming water-stable zwitterionic nitrogen-bas-CO_2 adducts, *Green Chem.*, 2019, **21**, 640–648.

98 M. D. Böhme, T. Eder, M. B. Röthel, P. D. Dutschke, L. F. B. Wilm, F. E. Hahn and F. Dielmann, Synthesis of N-Heterocyclic Carbenes and Their Complexes by Chloronium Ion Abstraction from 2-Chloroazolium Salts Using Electron-Rich Phosphines, *Angew. Chem., Int. Ed.*, 2022, **61**, e202202190.

99 L. Maresca, G. Natile, F. P. Fanizzi and F. Stasi, The bisphenanthrolinium ion. An X-ray crystal structure, *J. Am. Chem. Soc.*, 1989, **111**, 1492–1493.

100 R. V. Andreev, G. I. Borodkin and V. G. Shubin, Structure and Dynamics of the 1,10-Phenanthroline Complex with Nitrosonium Cation, *Russ. J. Inorg. Chem.*, 2001, **37**, 144–146.

101 D. F. Azar, H. Audi, S. Farhat, M. El-Sibai, R. J. Abi-Habib and R. S. Khnayzer, Phototoxicity of strained Ru(ii) complexes: is it the metal complex or the dissociating ligand?, *Dalton Trans.*, 2017, **46**, 11529–11532.

102 *Protonated 1,10-Phenanthroline as a Fluorescent Sensor for Fe(II) at Micro Molar Level Detections*, ed. G. Wijesekera, D. T. Arachchi, M. de Costa and R. Senthilnithy, From Innovation to Impact 2020, Colombo, Sri Lanka, 2020.

103 I. Despotović and R. Vianello, Engineering exceptionally strong oxygen superbases with 1,8-diazanaphthalene di-N-oxides, *Chem. Commun.*, 2014, **50**, 10941–10944.

104 S. Tshepelevitsh, A. Kütt, M. Lõkov, I. Kaljurand, J. Saame, A. Heering, P. G. Plieger, R. Vianello and I. Leito, On the Basicity of Organic Bases in Different Media, *Eur. J. Org. Chem.*, 2019, 6735–6748.

105 I. Kaljurand, A. Kütt, L. Sooväli, T. Rodima, V. Mäemets, I. Leito and I. A. Koppel, Extension of the self-consistent spectrophotometric basicity scale in acetonitrile to a full span of 28 pKa units: unification of different basicity scales, *J. Org. Chem.*, 2005, **70**, 1019–1028.

106 A. Kütt, S. Selberg, I. Kaljurand, S. Tshepelevitsh, A. Heering, A. Darnell, K. Kaupmees, M. Piirsalu and I. Leito, pKa values in organic chemistry – Making maximum use of the available data, *Tetrahedron Lett.*, 2018, **59**, 3738–3748.

107 P. Jutzi, C. Müller, A. Stammler and H.-G. Stammler, Synthesis, Crystal Structure, and Application of the Oxonium Acid [H(OEt2)2]+ [B(C6F5)4]–, *Organometallics*, 2000, **19**, 1442–1444.

108 P. Pyykkö and M. Atsumi, Molecular single-bond covalent radii for elements 1–118, *Chem. – Eur. J.*, 2009, **15**, 186–197.

109 P. Pyykkö and M. Atsumi, Molecular double-bond covalent radii for elements Li-E112, *Chem. – Eur. J.*, 2009, **15**, 12770–12779.

110 J. Ortmeyer, Y. Vukadinovic, A. Neuba, H. Egold, U. Flörke and G. Henkel, CCDC 1545124: Experimental Crystal Structure Determination, 2017.

111 H. Ferreira, M. M. Conradie, K. G. von Eschwege and J. Conradie, Electrochemical and DFT study of the reduction of substituted phenanthrolines, *Polyhedron*, 2017, **122**, 147–154.

112 B. N. Bandyopadhyay and A. Harriman, Photoreduction of 1,10-phenanthroline, *J. Chem. Soc., Faraday Trans. 1*, 1977, **73**, 663.

113 N. Armaroli, L. de Cola, V. Balzani, J.-P. Sauvage, C. O. Dietrich-Buchecker and J.-M. Kern, Absorption and luminescence properties of 1, 10-phenanthroline, 2, 9-diphenyl-1, 10-phenanthroline, 2,9-dianisyl-1, 10-phenanthroline and their protonated forms in dichloromethane solution, *J. Chem. Soc., Faraday Trans.*, 1992, **88**, 553.

114 N. Yoshikawa, S. Yamazaki, Y. Kakimoto, S. Eguchi, R. Yokoyama, N. Kanehisa, N. Tohnai, E. Nakata and H. Takashima, Emission properties of 1,10-phenanthroline derivatives induced by protonation of a nitrogen atom, *J. Mol. Struct.*, 2021, **1242**, 130728.

115 S. J. Lee, S. S. Lee, M. S. Lah, J.-M. Hong and J. H. Jung, Organic-inorganic hybrid nanomaterial as a new fluorescent chemosensor and adsorbent for copper ion, *Chem. Commun.*, 2006, 4539–4541.

116 B. Zhang, K.-S. Cao, Z.-A. Xu, Z.-Q. Yang, H.-W. Chen, W. Huang, G. Yin and X.-Z. You, Cell–Compatible Fluorescent Chemosensor for Zn 2+ Based on a 3,8-Extended 1,10-Phenanthroline Derivative, *Eur. J. Inorg. Chem.*, 2012, **2012**, 3844–3851.

117 Z. Aydin, A novel phenanthroline-based colorimetric turn-off optical sensor for Zn2+, *Inorg. Chim. Acta*, 2021, **517**, 120200.

118 Y.-Z. Han, G. Tian and Q. Yang, Two colorimetric and ratiometric fluorescence sensors for Zn^{2+} with 1,10-phenanthroline derivatives, *Inorg. Chem. Commun.*, 2023, **155**, 111105.

119 C. Bizzarri, C. Strabler, J. Prock, B. Trettenbrein, M. Ruggenthaler, C.-H. Yang, F. Polo, A. Iordache, P. Brüggeller and L. de Cola, Luminescent dinuclear Cu(I) complexes containing rigid tetraphosphine ligands, *Inorg. Chem.*, 2014, **53**, 10944–10951.

120 M. S. Henry and M. Z. Hoffman, Photophysics and photochemistry of aromatic nitrogen heterocycles. Fluorescence from 2,2′-bipyridine and 1,10-phenanthroline, *J. Phys. Chem.*, 1979, **83**, 618–625.

121 N. J. Hestand and F. C. Spano, Expanded Theory of H- and J-Molecular Aggregates: The Effects of Vibronic Coupling and Intermolecular Charge Transfer, *Chem. Rev.*, 2018, **118**, 7069–7163.

122 J. E. Yarnell, J. C. Deaton, C. E. McCusker and F. N. Castellano, Bidirectional "ping-pong" energy transfer and 3000-fold lifetime enhancement in a Re(I) charge transfer complex, *Inorg. Chem.*, 2011, **50**, 7820–7830.

123 M. W. Blaskie and D. R. McMillin, Photostudies of copper (I) systems. 6. Room-temperature emission and quenching studies of bis(2,9-dimethyl-1,10-phenanthroline)copper(I), *Inorg. Chem.*, 1980, **19**, 3519–3522.

124 S. Jensen, K. Tan, W. P. Lustig, D. S. Kilin, J. Li, Y. J. Chabal and T. Thonhauser, Structure-Driven Photoluminescence Enhancement in a Zn-Based Metal–Organic Framework, *Chem. Mater.*, 2019, **31**, 7933–7940.

125 Y. Li, L. Shi, L.-X. Qin, L.-L. Qu, C. Jing, M. Lan, T. D. James and Y.-T. Long, An OFF-ON fluorescent probe for Zn^{2+} based on a GFP-inspired imidazolone derivative attached to a 1,10-phenanthroline moiety, *Chem. Commun.*, 2011, **47**, 4361–4363.